Buckling of Helical Anchors Used for Underpinning

by
Robert Hoyt, M., ASCE
Gary Seider, A.M., ASCE,
Lymon C. Reese, Hon. M., ASCE, and
Shin-Tower Wang, M., ASCE

HUBBELL® CHANCE®
POWER SYSTEMS

Printed in USA

Bulletin 01-9605
RG 2/96

BUCKLING OF HELICAL ANCHORS USED FOR UNDERPINNING

by

Robert Hoyt[1], M., ASCE, Gary Seider[1], A. M., ASCE,
Lymon C. Reese[2], Hon. M., ASCE, and
Shin-Tower Wang[2], M., ASCE

ABSTRACT

Helical anchors have been used in various applications, including the underpinning of distressed foundations for either stabilization or rehabilitation. In such applications, the possible buckling of the slender shaft under eccentric, compression loading is of interest. The authors have studied this phenomenon using full-scale load tests and computer modeling to determine under what conditions buckling is a practical concern. Prior to computer solutions, however, laboratory testing of the underpinning bracket assembly was required. Brackets were attached to a concrete block and axial loads were applied in increments with a typical jacking arrangement. Careful measurements then yielded the rotational characteristics of the bracket. The anchor system was then modeled, using the finite-difference technique as implemented in the program LPILE^{PLUS}. Buckling loads were computed for helical anchor shafts of different sizes and lengths in soils of various strengths, with the lateral response of the soil represented by nonlinear p-y curves. Full-scale, field loading tests were conducted in both granular and cohesive

[1]A. B. Chance Co., 210 N. Allen St., Centralia, MO 65240

[2]Lymon C. Reese & Assoc., Inc., PO Box 180348, Austin, TX 78718

soils and the results found to be in agreement with the computer simulations. The results of the computer modeling, confirmed by the field loading tests, indicated that buckling, either linear or nonlinear, is of practical concern only for long anchor shafts in the softest soils. This is in agreement with past findings regarding conventional pile foundations. Data are presented which allow a preliminary determination of whether buckling might be a practical concern for a given application. In these cases, load tests or computer simulation using the modeling techniques developed for this study can be used to predict buckling loads and the design can be adjusted accordingly.

INTRODUCTION

Helical anchors, also known as screw anchors, consist of one or more helically shaped plates attached to a central shaft. They are twisted into the ground using any convenient method from a hand wrench to vehicle mounted drilling equipment. Historically, helical anchors have been used mainly as tension anchors for electric transmission line support structures, but they have also been used successfully to resist compression and lateral loads.

An important compression application of helical anchors is in the underpinning of distressed foundations for stabilization against further damage or remediation (Figure 1). Typically, anchors used in such applications have either a 38 mm or 44 mm (1-1/2" or 1-3/4") round-cornered square solid steel shaft. The shaft length may vary as necessary to get the helical bearing plate(s) embedded into competent soil, typically 2 to 3 m (7 to 10 ft) but sometimes as much as 15 m (50 ft) and never less than 1.5 m (5 ft). Slenderness ratios (L/R) in the 100 to 200 range are thus typical, making buckling of the shaft a matter of some concern. Mitigating factors include the fact that the loads are typically a small fraction (less than 1/4) of the shaft's compressive yield load and the restraint provided at the top of the shaft (by the bracket) and along the shaft (by the soil). The necessity of coupling together several short shafts when overhead clearance is small, or depths greater than 3 m are required, may heighten the susceptibility to buckling due to the looseness of the fit at the couplings. These factors combine to take buckling analysis of helical anchors in underpinning applications out of the realm of the simple Euler equation.

The typical helical anchor underpinning system consists of a helical anchor and a foundation bracket assembly installed

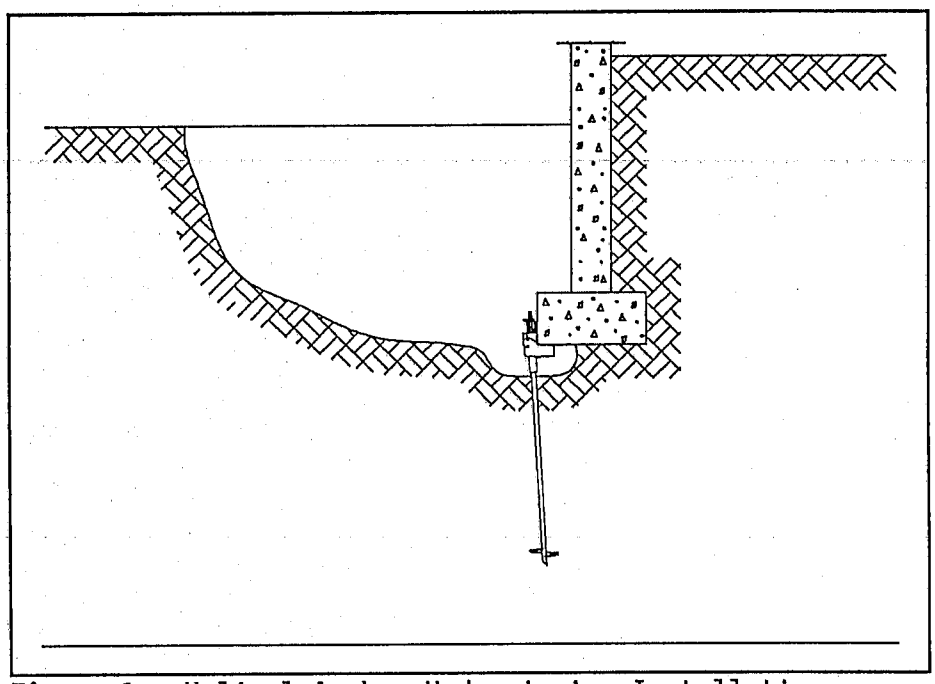

Figure 1: Helical Anchor Underpinning Installation

in a temporary excavation next to the distressed foundation. The helical anchor shown in Figure 1 is a single helix type with a one-piece shaft, but multiple helices and/or extension shafts may be used depending on site conditions and required load capacity. The bracket assembly (Figure 2) consists of two major parts (a foundation bracket and a T-pipe) and some fasteners. The bracket is bolted to the face of the foundation with its lip extending under and in contact with the foundation bottom. The anchor shaft extends up between the bracket's gussets. The T-pipe slides over the anchor shaft and is partially restrained by the welded brace and a cross-bolt (Figure 3). In this configuration, the T-pipe can slide freely upward along the anchor shaft. Other motions are restrained by either the bracket or the anchor. The T-pipe can be prevented from sliding up by tie bolts passing through the T-pipe flange and ears provided on the bracket as shown in Figure 2. This is the configuration used for foundation stabilization, where it is not intended to jack the foundation back to its original position. Any load the foundation puts on the bracket is transmitted to the anchor through tension in the tie bolts.

HELICAL ANCHOR UNDERPINNING SYSTEM

The same system can be used with a reusable jack and jacking frame to remediate the foundation (Figure 4). In

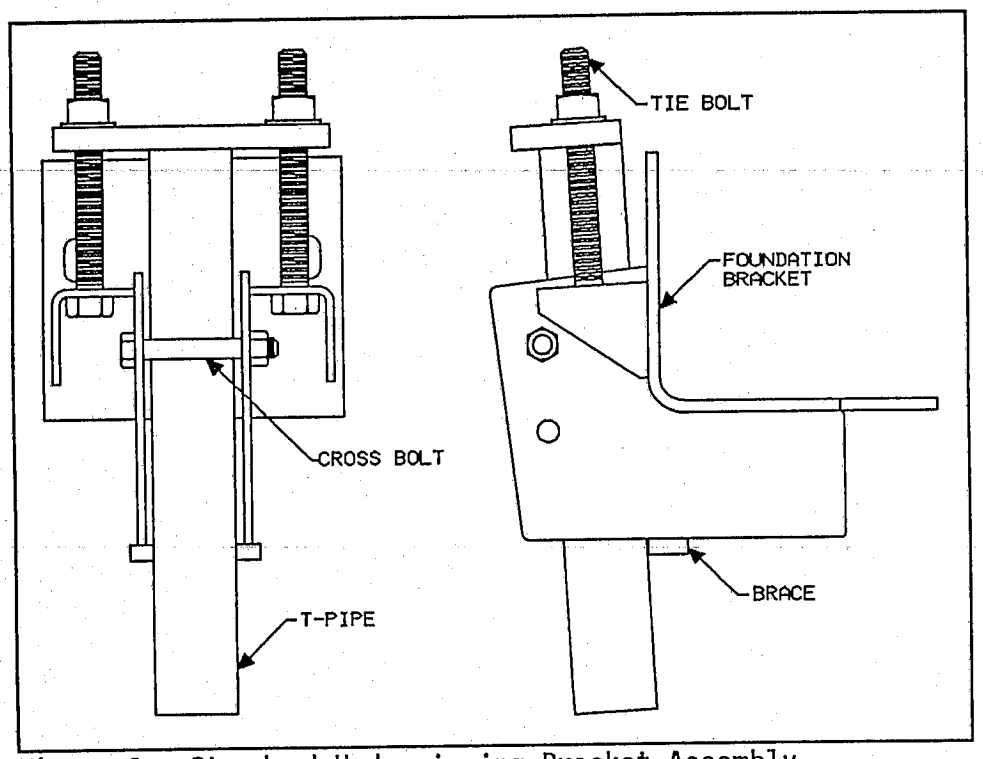

Figure 2: Standard Underpinning Bracket Assembly

this configuration, the tie bolts pass freely through the T-pipe flange to connect the bracket to the jacking frame via extension bolts and couplings. Once the foundation has been lifted, the tie bolt nuts can be locked off against the top surface of the T-pipe flange and the jack and jacking frame removed.

Once the tie bolt nuts are locked off, the bracket/anchor assembly is able to support the foundation. If the foundation/ bracket/T-pipe/anchor shaft assembly were rigid, the computer model could be restricted to just that portion of the anchor shaft below the lower end of the T-pipe, with fixed end conditions (deflection y_t and slope $s_t = 0$) at the "top." The lateral shear P_t and the axial load Q would be input values, while the moment M_t at the top would be calculated by the software (Figure 5). However, neither the bracket/foundation rotational joint nor the bracket/T-pipe translational joint nor the T-pipe/anchor shaft rotational joint is rigid within the working load range.

The load path from the bracket to the T-pipe consists of tension in the tie bolts. Any such tension produces clockwise moment on the foundation bracket when viewed from the side as in Figure 3. In the absence of the anchor shaft, this would cause the bracket to rotate clockwise until the

resisting moment due to bending of the bracket offset the imposed moment. With the anchor shaft in place, the brace imposes a lateral load on the T-pipe which in turn puts a "kick-out" force on the anchor shaft. Bracket rotation ceases when the combined moments due to bracket bending resistance and the anchor shaft's reaction on the T-pipe and brace offset the moment due to the tie bolt tension.

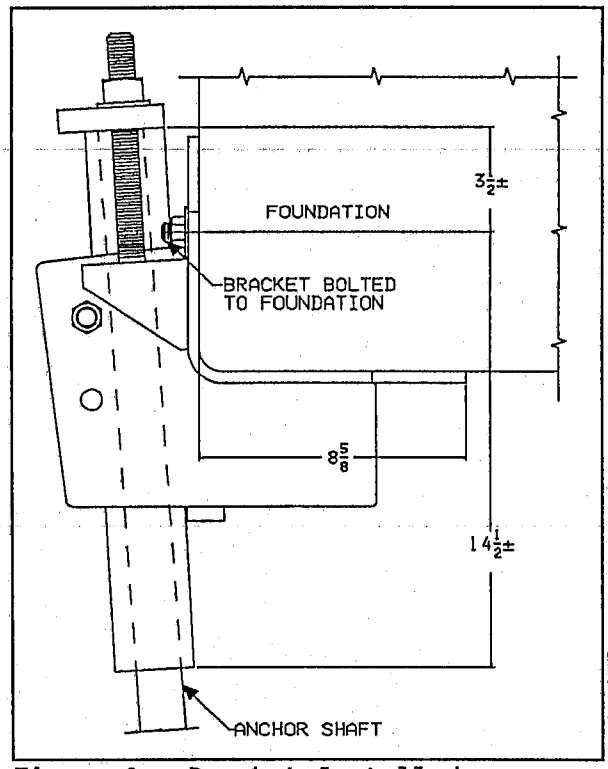

Figure 3: Bracket Installed on Foundation & T-Pipe on Anchor

As load is transferred to the anchor, it and the T-pipe move axially with respect to the bracket. This introduces frictional forces, f_{brace} and f_{xbolt} at the welded brace and cross-bolt, respectively (Figure 6). In foundation stabilization applications, these frictional forces are inconsequential since they only reduce the load Q_{tie} in the tie-bolts. In the case of remediation, however, it is common to measure the jacking load Q_{jack} and important to realize that some of the jacking load (as much as 20%, according to test results) is resisted by this friction and does not reach either the anchor or the foundation (Q_{anchor} and Q_{fdn}, respectively). The equations of statics shown in Figures 6 and 7 assume that Q_{anchor} and Q_{fdn} are oriented the same, of course. While this cannot be expected, the equations nevertheless serve to show in a qualitative way the effects of the frictional forces.

In general, the end of the anchor shaft does not perfectly match the underside of the T-pipe flange. This is due to imperfect cutoff in the manufacture of the shaft as well as field misalignment. Therefore, the load tends to be transferred along one of the edges of the shaft end. This and the T-pipe kick-out force described above cause the shaft to bend within the loosely fitting T-pipe, resulting in rotation of the shaft with respect to the T-pipe.

BUCKLING ANALYSIS BY FINITE DIFFERENCES

One way to determine the buckling load of a helical anchor in an underpinning application is to model it as a beam-column on an elastic foundation. The finite difference technique can then be used to solve the governing differential equation for successively greater loads until, at or near the buckling load, failure to converge to a solution occurs.

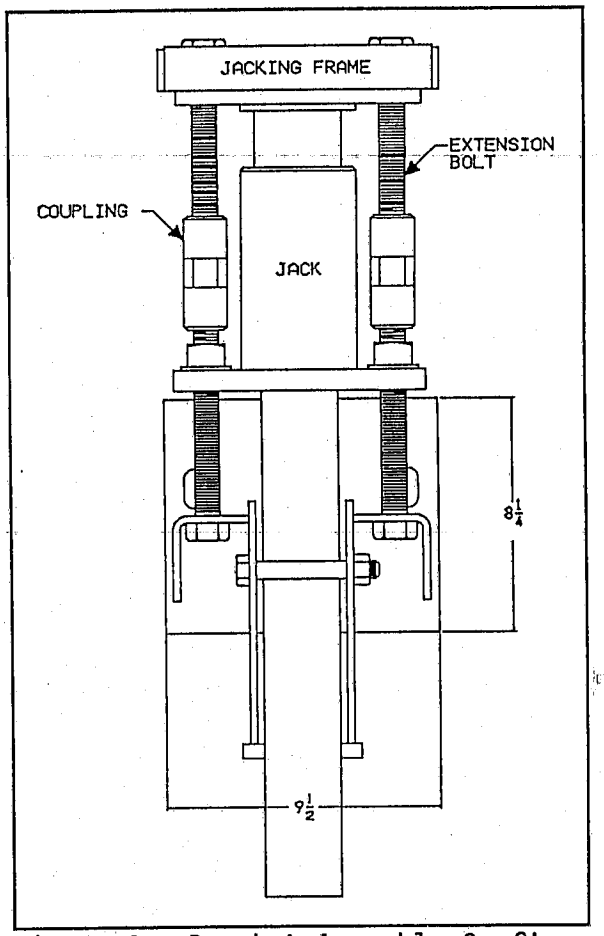

Figure 4: Bracket Assembly Configured for Remediation

The derivation for the differential equation for the beam-column on a foundation was given by Hetenyi (1946). The assumption is made that a bar on an elastic foundation is subjected not only to lateral loading, but also to a compressive force Q acting at the center of gravity of the end cross-sections of the bar, leading to the differential equation

$$EI\frac{d^4y}{dx^4} + Q\frac{d^2y}{dx^2} + E_s y = 0 \qquad (1)$$

where y is the lateral displacement, x is the distance along the axis, EI is the bending stiffness, and E_s is the secant modulus of the soil response curve. If a distributed lateral load w acts along some portion of the shaft length, the final equation becomes

$$EI\frac{d^4y}{dx^4} + Q\frac{d^2y}{dx^2} + E_s y + w(x) = 0 \qquad (2)$$

Closed form solution of this equation is possible for some simplified cases, but for general applications, formulation of equation (2) in numerical terms for computer solution is advantageous (Reese, 1971). Some advantages of a general purpose computer solution are:

The bending stiffness EI of the beam-column can be varied along its length. This variation may be due to changes in material or geometry along the length, or to stress effects.

The soil secant modulus can vary from point to point along the beam-column's length and, at a given point, as a function of deflection.

The effect of the axial load on deflection and bending moment can be considered and buckling problems can be solved.

The effect of the axial load Q is most obvious in the second term of the differential equation (the secondary moment). However, the axial load also affects combined stress. Once the combined stress at a point exceeds the yielding level, the flexural rigidity of the section will decrease, which effect shows up in the first term of equation (2). This causes more deflection, which affects the third term and all the derivatives of y with respect to x. The increased deflection generates more secondary moment, leading to yet another round of effects. While Q has a direct effect on combined stress, its effect on deflection is much less pronounced so that the process is stable for loads below some critical value. The beam column is unable to support loads above the critical due either to elastic (Euler) buckling or the formation of a mechanism of plastic hinges.

To define the critical load for a particular structure using the finite difference technique, it is necessary to analyse the structure under successively increasing loads. This is necessary because the solution algorithm becomes unstable at loads above the critical. This instability may be seen as a convergence to a physically illogical configuration or failure to converge to a solution at all. Since physically illogical configurations are not always easily recognized, it is best to build up a context of correct solutions at low loads with which any new solution can be compared.

DATA COLLECTION AND ANALYSIS

The general method used in this study was to utilize the finite difference technique to analyze various lengths of shaft embedment in soils of various strengths. Limit loads were determined and then the results were validated by comparing them to actual field test data. Once the results were validated, they were used to prepare charts enabling the designer to check specific applications for buckling susceptibility.

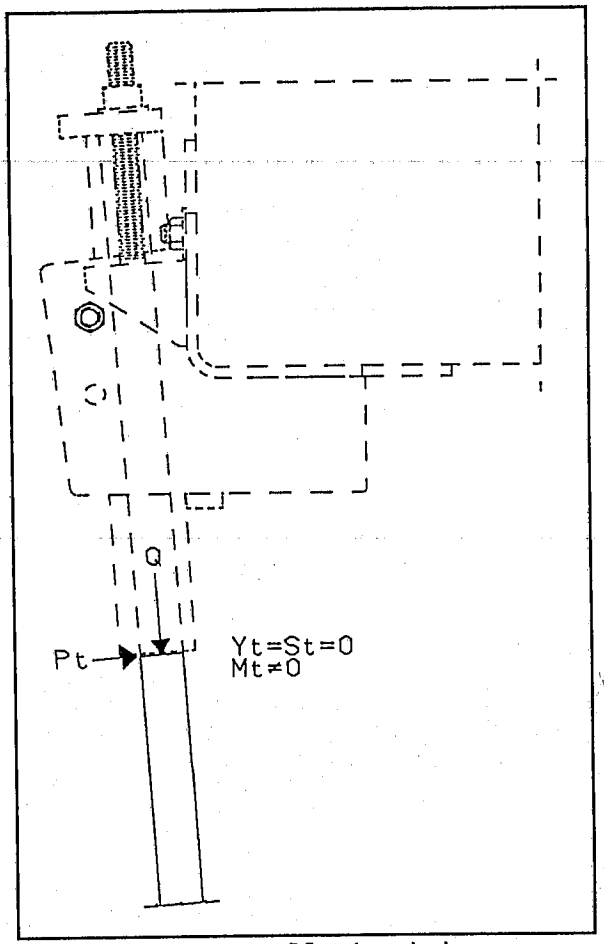

Figure 5: Laterally Loaded Pile Model (Rigid Bracket)

The particular computer program used was developed for analysis of laterally loaded piles. Two useful features of this software are algorithms to generate p-y curves from soil property and stratification data and the ability to handle piles whose stiffnesses vary with depth and axial load. There were some drawbacks to its use for this particular project, however, in that the available pile top boundary conditions did not include the particular conditions imposed by the typical helical anchor underpinning bracket assembly. A method was devised to model the conditions utilizing the input distributed lateral load capability of the software. Since the charts presented herein do not allow comprehensive determination of the buckling susceptability of all applications, the method is described in some detail for the benefit of those who may be faced with the necessity of conducting similar analyses.

Since the program models only the pile and soil, the effects of the foundation, bracket and T-pipe on the pile must be modeled with boundary conditions. The boundary conditions chosen for this study were specified lateral

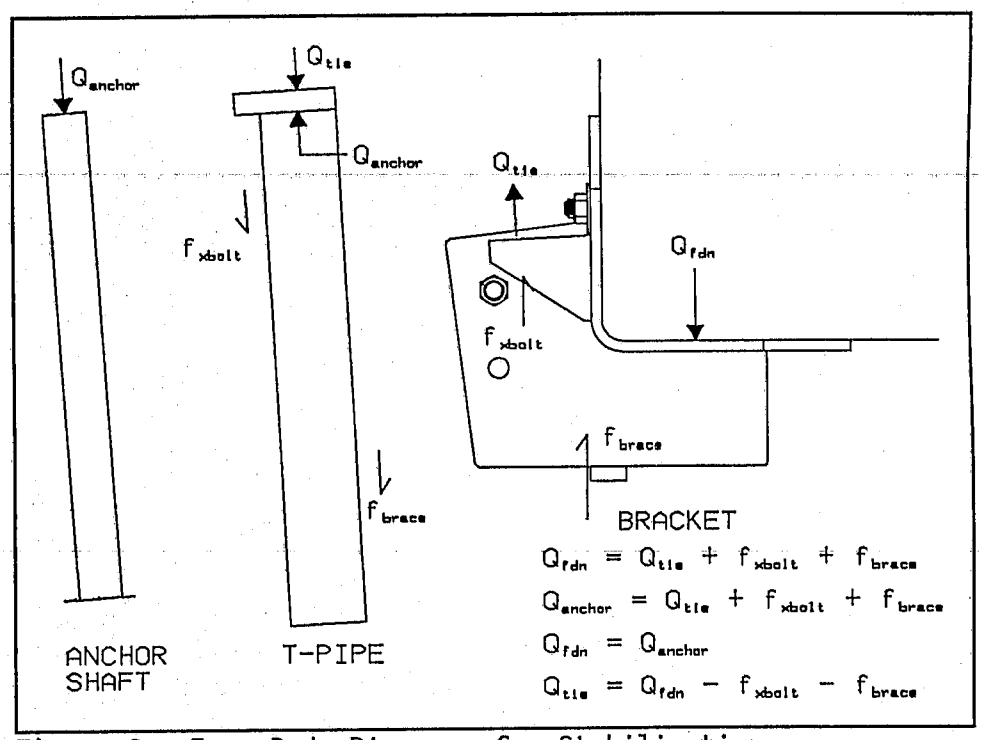

Figure 6: Free Body Diagrams for Stabilization

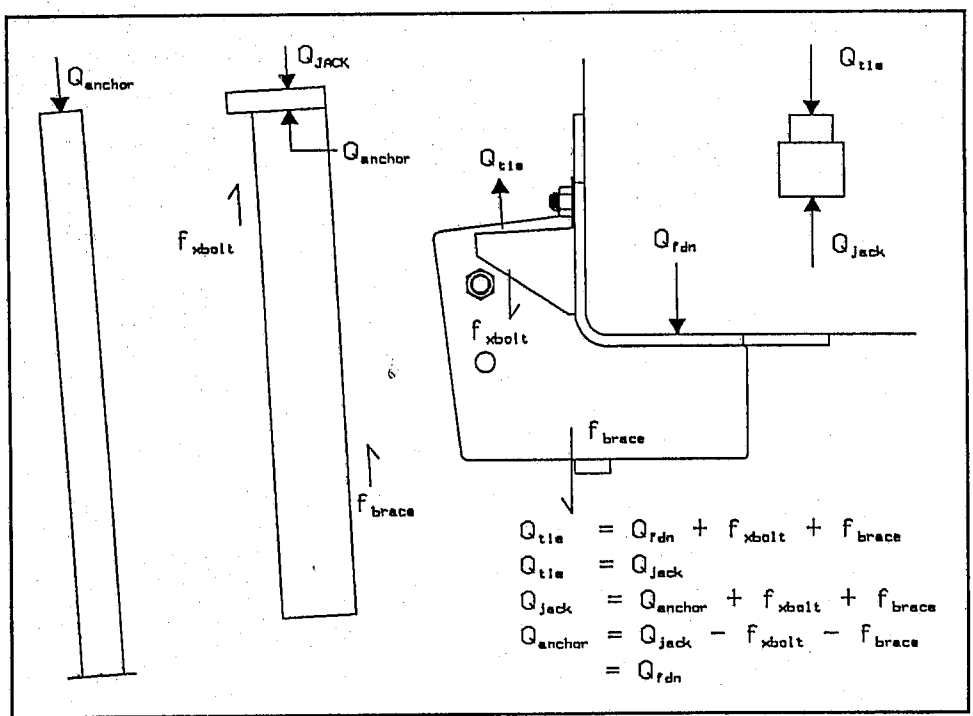

Figure 7: Free Body Diagrams for Remediation

displacement (y_t), axial load (Q) and moment (M_t) at the top, where the anchor shaft contacts the bottom of the T-pipe flange plate (Figure 8). The lateral displacement y_t is a function of the axial load and the position of the T-pipe

within the bracket. Previous laboratory and field testing have shown that the T-pipe and portion of the bracket below the foundation attachment bolts tend to rotate as a rigid body about a yield line passing through the attachment bolts. It can be seen from the dimensions given in Figure 3 that under such conditions y_t will be about 25% of the displacement of the lower end of the T-pipe and in the opposite direction. Sensitivity analysis showed the solution to be relatively insensitive to the value specified, so a constant value of 2.5 mm was used for most analyses. The axial load Q is, of course, the independently imposed load and the moment M_t is a function of Q and the position of contact between the anchor shaft end and the T-pipe flange plate. For this study, contact was assumed to be at one or the other worst-case position such that

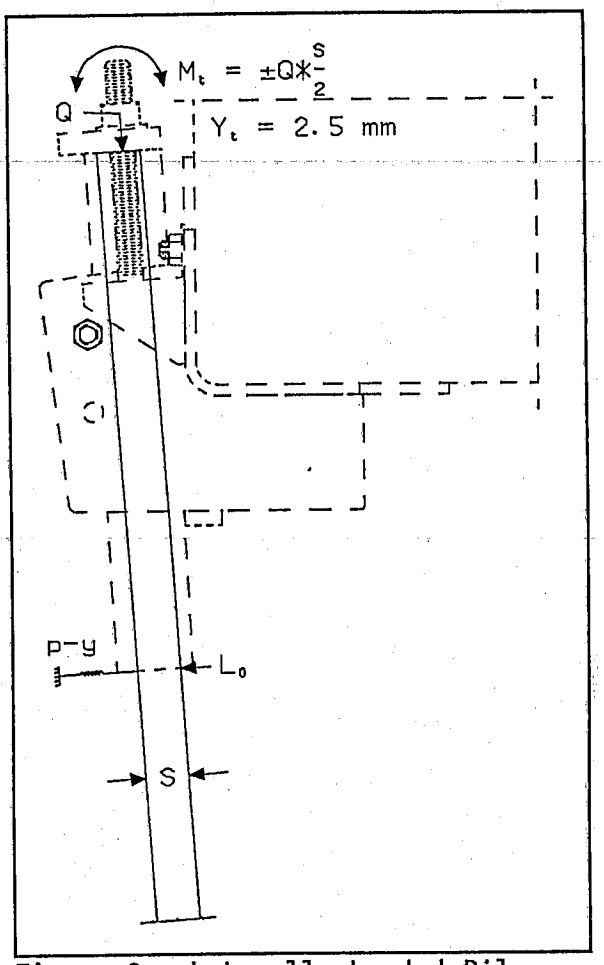

Figure 8: Laterally Loaded Pile Model (Flexible Bracket)

$$M = \pm Q \frac{S}{2}$$

where s is the size of the square shaft across flats.

The effect of bracket flexibility was modeled by using distributed lateral load and input p-y curve modeling capabilities. The T-pipe kick-out force due to bracket rotation was modeled using an input distributed lateral load (W) which was defined so that it only acted on one shaft node. This load was opposed by an input p-y relation which, as the shaft moves laterally, generates an opposite load on the same node to model the effect of increasing bending resistance in the bracket. The values to be input were

determined from a laboratory test of the bracket assembly mounted on a concrete test fixture.

This laboratory test setup is depicted in Figure 9. As the axial load is increased, the bracket and T-pipe tend to rotate clockwise but are restrained from doing so by the strain-gaged load cell. The load cell is mounted such that its movement, and thus the movement of the T-pipe and bracket, can be controlled. During the test, the load was first varied from zero to 178 KN (40k, twice the rated load of the bracket) in 22 KN (5k) increments, with the deflection of the T-pipe as indicated on the dial indicator being held to zero. The restraining load provided by the load cell for each applied axial load was measured. The procedure was then repeated with an increasing value of deflection at the dial indicator being imposed for each series of axial loads. The result was a series of restraining loads vs deflections for each value of applied load (Figure 10).

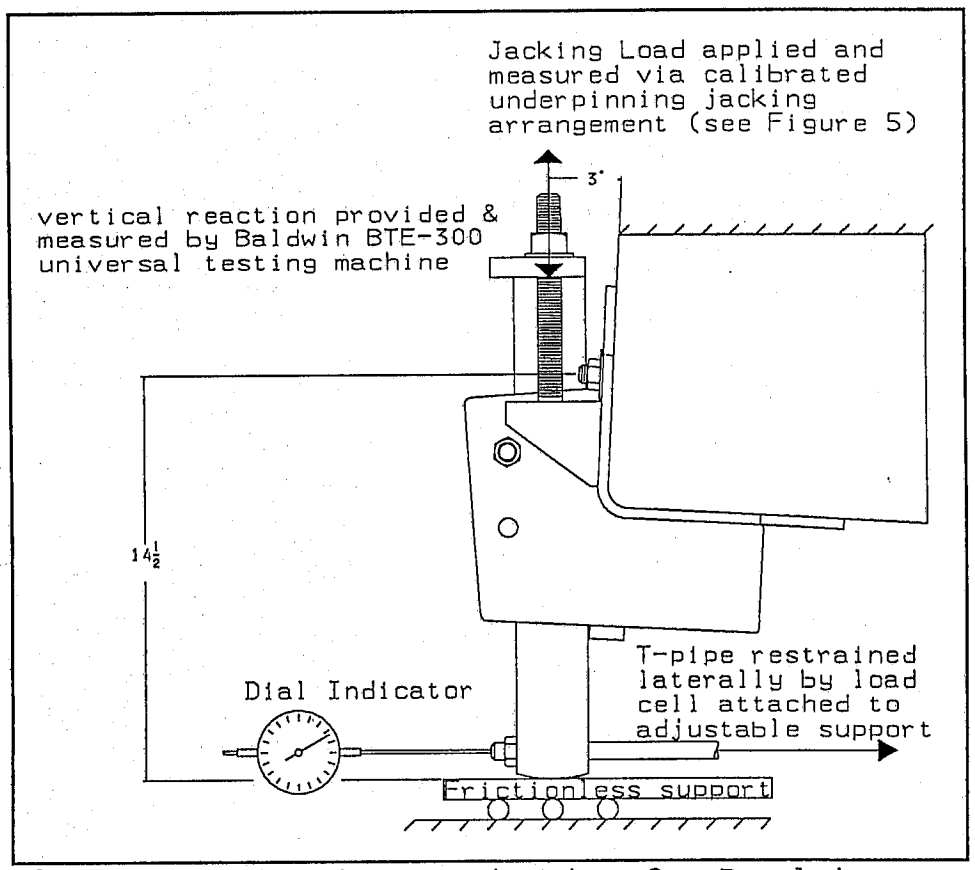

Figure 9: Laboratory Test Setup for Bracket Stiffness Measurement

For a given axial load, the "distributed" lateral load used in computer modeling was that which was necessary to produce a lateral nodal load equal to the restraining load

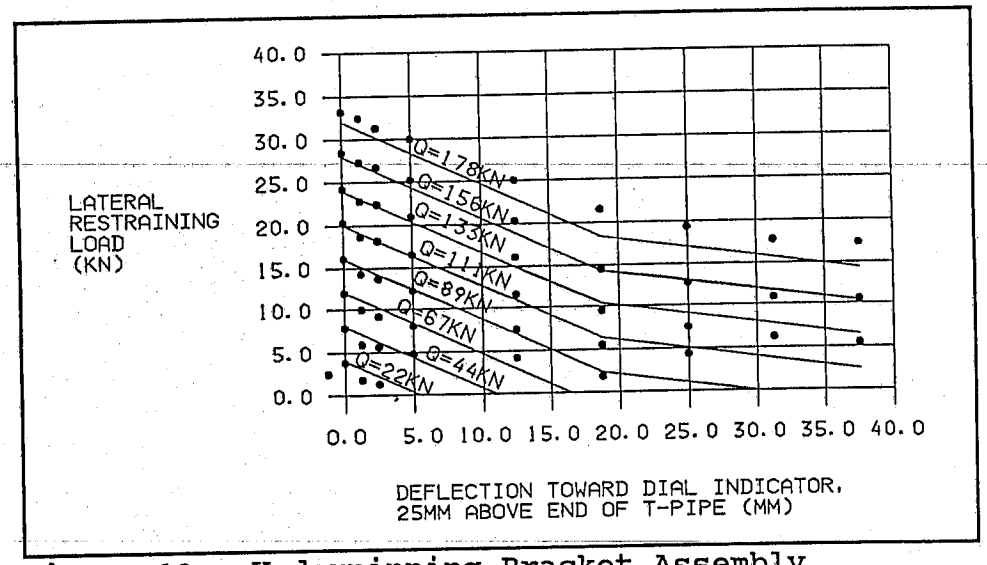

Figure 10: Underpinning Bracket Assembly Stiffness Data

measured in the laboratory test at zero deflection. The sign convention used was such that a negative value was required to correspond with the configuration shown in Figure 3. This load will "follow" the anchor shaft, maintaining a constant value regardless of lateral deflection, so it was necessary to provide some means of moderating it to model the increased bracket bending resistance with deflection. This was accomplished with an input p-y relation at the same node. The input y values could be those values of deflection which were imposed on the lower end of the T-pipe during the laboratory test, with the p value for each y value being such that the "soil" reaction will reduce the net lateral load at the node to the value which was measured in the laboratory test. However, the test data showed a consistent stiffness of 795 KN/m (4545 lb/in), at all values of the axial load, for deflections less than 19 mm (0.75 in) and 230 KN/m (1313 lb/in) for deflections above 19 mm, so these stiffnesses were used to generate the input p-y curves for the computer runs.

For a given axial load Q,

$$w\ (F/L) = -\frac{L_0}{x_{final} - x_{initial}},\quad where$$

L_0 = Load (F) measured in laboratory test at zero deflection,

$x_{initial}$ = distance (L) along shaft to starting point of distributed load, and

x_{final} = distance (L) along shaft to ending point of distributed load

Then for each value of deflection y,

$$p\ (F/L) = \frac{L_0 - L_y}{x_{final} - x_{initial}},\quad where$$

L_y = Load (F) measured in laboratory test at y deflection

If x_i is the value of x at the node closest to where the bottom of the T-pipe contacts the anchor shaft, x_{i-1} is the x value at the nearest node above it and x_{i+1} is the value at the nearest node below it, then meeting the conditions

$$x_{i-1} < x_{initial} < x_i$$

$$and \qquad (6)$$

$$x_i < x_{final} < x_{i+1}$$

will cause the distributed lateral load and p-y relation to affect only the desired node.

The particular computer program used had two other features which had to be addressed for use in this project. First, routines were provided to calculate the moment vs stiffness (EI) relations for given axial loads of steel pipe and various reinforced concrete sections. However, neither round-cornered nor square-cornered square solid sections were included. This was handled by revising the code to allow direct input of moment-stiffness relations which had been calculated separately (Figure 11). Second, the algorithms for calculating p-y relations in stratified soils were arranged such that input p-y curves at lesser depths affected the internally calculated p-y relations for greater ones. This made it difficult to model the 0.5 m (20 inch) free length and the bracket stiffness described above without affecting the p-y relations generated for true soil contact. This was eventually handled by generating and printing out the p-y curves in preliminary runs, then inputting those same p-y curves directly for depths greater than the 0.5

m depth of the excavation.

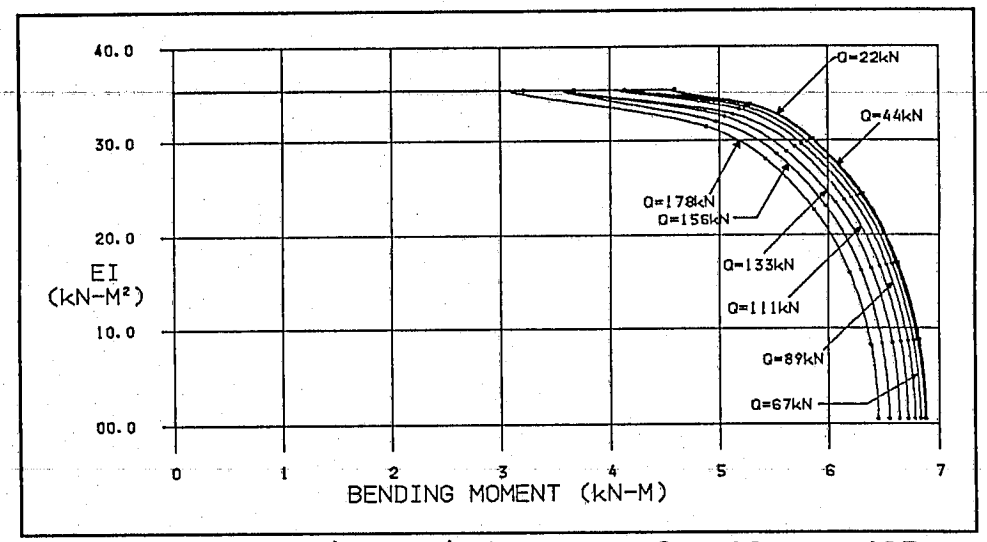

Figure 11: Bending Stiffness EI for 38 mm, 497 MPa Square Bar

RESULTS

Results of several full-scale underpinning load tests were reported by Seider (1993). In one of these tests, a helical anchor of the type ("SS5") investigated in this project was used. This test was modeled using the revised software with good results, i.e., the maximum moments were comparable, and they occurred at approximately the same depth, and the solution was stable over the range of loads that was actually applied. Two new full-scale load tests were also performed with more extensive strain-gaging of the shafts. In these two tests, a large (about 1 m cube) concrete block was anchored down on the ground surface to provide the bracket mounting surface and reaction. One test was conducted in clay in Centralia, MO (soil profile similar to that reported by Seider) and the other test was in uniform sand in Leadwood, MO. This test was on the same site (Eaton Dam) as that used by Clemence, et al (1994). Actual test data is compared to the computer results in Table I for all three tests. Data is given for loads Q in approximately 44 KN (10k) increments, with the actual test results in the first row and the computed results in the second row for each load Q. In the table, $M_{x=0.47}$ is the bending moment at the end of the T-pipe, $x_{M=0}$ is the distance along the shaft where the bending moment first reaches zero and $M+_{max}$ is the

maximum positive bending moment. The last column (labeled @x=) gives the distance along the shaft where $M+_{max}$ occurs.

Table I: Actual vs Computed Bending Moments for Full Scale Load Tests

Q (KN)	$M_{x=0.47}$ (KN-m)	$x_{M=0}$ (m)	$M+_{max}$ (KN-m)	@x= (m)
	First Centralia, MO Test (Seider, 1993)			
40.0	-2.15	1.09	0.565	1.55
	-2.28	1.09	0.610	1.60
89.8	-2.15	1.07	1.58	1.55
	-6.49	1.30	4.11	1.88
	Second Centralia, MO Test			
42.2	-1.08	1.64	NA	2.01+
	-1.22	0.762	0.279	0.940
87.1	-2.50	1.38	NA	2.01+
	-3.13	0.787	.860	1.07
137	-5.14	1.12	1.08	1.66
	-6.37	0.940	2.79	1.35
	Leadwood, MO Test			
39.3	-1.94	NA	NA	1.93+
	-1.28	0.787	0.268	1.02
79.9	-4.31	1.89	NA	1.93+
	-2.48	0.813	0.723	1.07

In the table, $M+_{max}$ is listed as NA (Not Available) in some cases because the maximum positive moment did not occur in the strain-gaged section. Also, $x_{M=0}$ is listed as NA for the 39.3KN load at Leadwood because the moment was negative for the entire strain-gaged section. It will be seen that in all three cases the computed moment curves differ from the experimental ones sufficiently to bear further investigation.

Next, computer runs were made for various loads and shaft lengths in six different clay strengths and five different sand densities. The basic soil property data used is given in Table II, where N is the blow count per

ASTM-D1586, P-Y Code is a software-specific input value which determines the p-y curve generation algorithm that was used, Cu is one-half the unconfined compressive strength, Phi is the angle of internal friction, Gamma is the dry unit weight, e50 is the strain corresponding to one-half the maximum principal stress difference in an undrained shear test, and Ks is the horizontal subgrade modulus. A P-Y Code of 1 implies p-y curves for soft clay using the criteria of Matlock (1970) were generated, while a P-Y Code of 2 implies p-y curves for stiff clay using the Reese et al (1975) criteria and 4 implies p-y curves for sand using the criteria of Reese et al (1974). The soil property data was not varied with depth. The results of these runs are depicted graphically in Figure 12.

Table II: Soil Parameters Used in Computer Analyses

Description	N	P-Y Code	Cu (kPa)	Phi (deg)	Gamma (kN/m^3)	e50	Ks (MN/m^3)
Clays							
Very Soft	1	1	9.58	0.	12.9	0.060	8.
Soft	3	1	19.2	0.	13.5	0.020	27.
Medium	6	1	38.3	0.	14.4	0.010	136.
Stiff	12	3	71.9	0.	16.3	0.005	271.
Very Stiff	24	3	143.	0.	18.8	0.004	542.
Hard	32+	3	287.	0.	20.7	0.0035	1085.
Sands							
Very Loose	2	4	0.	28.	11.0	0.	1.
Loose	7	4	0.	29.	15.1	0.	7.
Medium	20	4	0.	33.	17.3	0.	24.
Dense	40	4	0.	38.5	20.4	0.	61.
Very Dense	50+	4	0.	43	22.8	0.	92.

The two dashed lines in Figure 12 represent the previously mentioned minimum installed shaft length of 1.5 m (5 ft) and bracket assembly strength limit of 178 kN (40 K). Configurations outside these limits were not investigated since they are not of practical interest. The areas to the right of and below the various labeled solid lines define regions where convergence to a physically logical solution always occurred. Conversely, the areas to the left of and above these boundaries define regions where convergence to illogical solutions and failure to converge at all were encountered. Where the boundary is inclined, an increase in shaft length will result in an increase in axial load capacity due to the increased area available to develop lateral resistance. The horizontal portions of the "Very

Soft Clay" and "Soft Clay" boundaries represent true buckling limits. In very soft clay, the shaft buckled elastically while in soft clay it first yielded and then buckled inelastically. No buckling of either type was encountered for any of the other soil conditions.

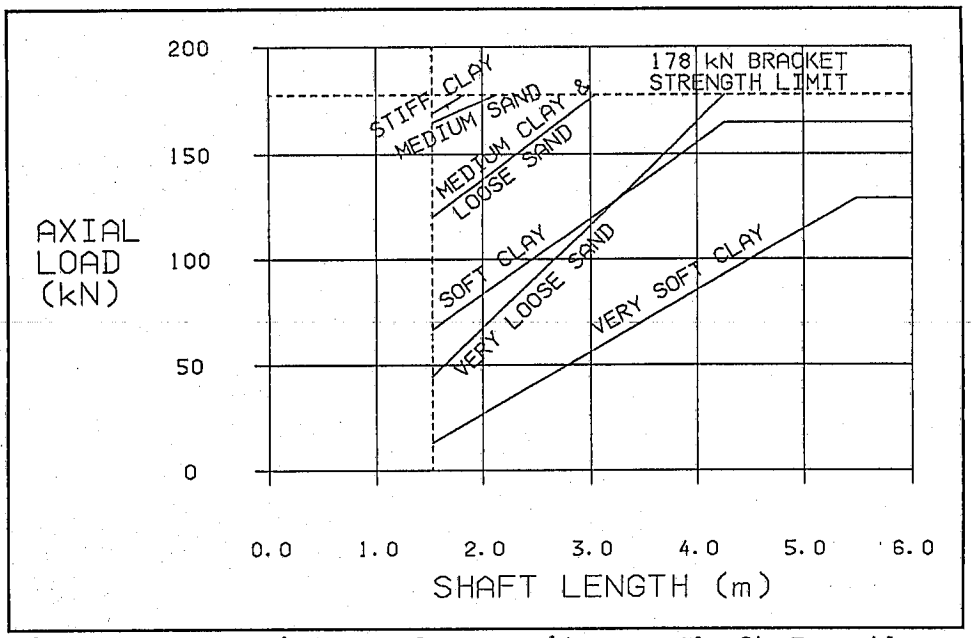

Figure 12: Axial Load Capacity vs Shaft Length for Various Soils

The convergence problems encountered in the areas to the left of and above the boundaries are illustrated in Figure 13. All the deflection curves were obtained at an axial load of 129 kN in very soft clay. Curve (a) was obtained with a shaft length of 0.61 m and represents a shaft which is too short to effectively resist the T-pipe kick-out force.

At a length of 0.76 m, the solution failed to converge at all. Curve (b) was obtained at a length of 0.91 m and is clearly illogical for the applied forces. Failure to converge was again encountered at a length of 1.12 m, while illogical curve (c) occurred at 1.22 m. At 1.68 m curve (d) occurred, followed by curves (e) at 2.24 m and (f) at 3.05 m with no intervening convergence failures. A relatively large interval of continuous convergence failures followed before the region of continuous convergence success was reached (curve (g), 5.49 m). Note that the deflections of curves (d) through (g) have been scaled up by a factor of 5 for clarity.

Curves (b) through (f) are termed "illogical" because at least some part of the shaft is seen to have deflected

opposite to expectation. This is most obvious in curves (b) and (c). Of course, one must ask whether it is the expectation which is invalid rather than the solution, since the solution is at least known to obey the laws of mechanics. If these curves did represent valid solutions, then solutions would also exist for all lesser loads on shafts of the same length in the same soil. Such is not the case for the examples or for solutions in general in the areas of the chart to the left of and above the various boundary lines.

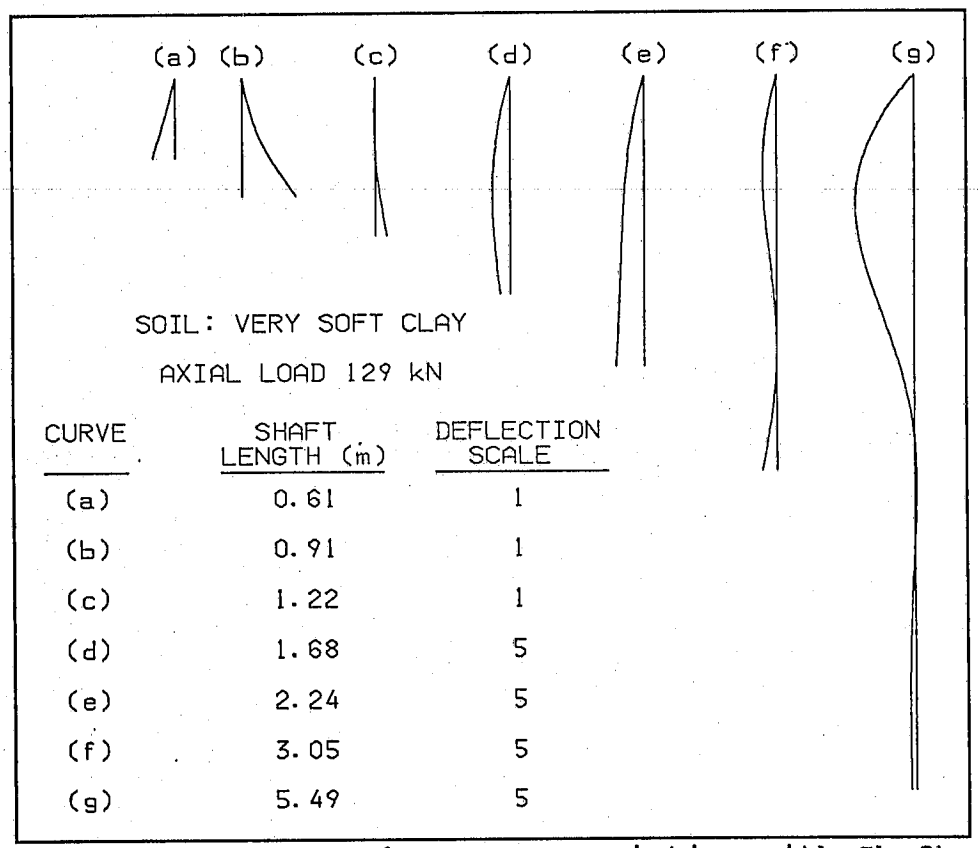

CURVE	SHAFT LENGTH (m)	DEFLECTION SCALE
(a)	0.61	1
(b)	0.91	1
(c)	1.22	1
(d)	1.68	5
(e)	2.24	5
(f)	3.05	5
(g)	5.49	5

Figure 13: Deflection Curve Variation with Shaft Length

CONCLUSIONS

Computer modeling of the three full-scale load tests showed good, but not complete agreement, with the experimental data. Two possible sources of error are the effects of the anchor shaft couplings on the shaft stiffness and the soil resistance. The couplings fit together loosely, forming a local moment-free area for small rotations. Once the free rotation has been used up, the stiffness of the coupled area is about the same as for the rest of the shaft. Also, the coupling opens up a larger hole than the rest of the shaft

can fill, so an annular space is left within which there is no shaft/soil contact. No attempt was made to model either of these effects. Further investigation is needed in this area.

The modeling showed that buckling is a practical concern only in the softest soils, and this is in agreement with past analyses and experience on other types of piles (Sowers and Sowers, 1970). Figure 12 can be used to determine whether a particular application is clearly stable (well to the right and below the applicable boundary line), clearly unstable (well to the left of or above the boundary), or questionable (in the vicinity of the boundary). Load tests can be used to resolve questionable applications.

Further work is planned to investigate the effects of soil stratification and shaft couplings.

REFERENCES

Clemence, S. P., Crouch, L. K., and R. W. Stephenson (1994), "Prediction of Uplift Capacity for Helical Anchors in Sand", 2nd International Geotechnical Conference, Cairo, Egypt, Vol. I, pp 332-343.

Hetenyi, M. (1946), Beams on Elastic Foundation, The University of Michigan Press, Ann Arbor, MI, p 127.

Matlock, H. (1970), "Correlations for Design of Laterally Loaded Piles in Soft Clay," Proceedings, Second Annual Offshore Technology Conference, Holuston, TX, pp 577-594.

Reese, L. C. (1971), "The Analysis of Piles Under Lateral Loading", Proceedings, Symposium on the Interaction of Structure and Foundation, The Midland Soil Mechanics and Foundation Engineering Society, University of Birmingham, England, pp 206-218.

Reese, L. C., Cox, W. R., and Koop, F. D. (1974), "Analysis of Laterally Loaded Piles in Sand," Proceedings, Offshore Technology Conference, Houston, TX, pp 473-484.

Reese, L. C., Cox, W. R., and Koop, F. D. (1975), "Field Testingand Analysis of Laterally Loaded Piles in Stiff Clay," Proceedings, Offshore Technology Conference,

Houston, TX, pp 671-690.

Seider, G. (1993), "Eccentric Loading of Helical Piers™ for Underpinning", Proceedings, Third International Conference on Case Histories in Geotechnical Engineering, St. Louis, MO, pp 139-145.

Sowers, G. B. and G.F. Sowers (1970), Introductory Soil Mechanics and Foundations, Third Edition, Macmillan Publishing Co., New York, NY, p 454.